Journal of Modern Optics
Publication details, including instructions for authors and subscription information:
http://www.informaworld.com/smpp/title~content=t713191304

Infrared wavelength-dependent optical characterization of NbN nanowire superconducting single-photon detectors

Martin J. Stevens [a]; Robert H. Hadfield [b]; Thomas Gerrits [a]; Tracy S. Clement [a]; Richard P. Mirin [a]; Sae Woo Nam [a]
[a] Optoelectronics Division, National Institute of Standards and Technology, Boulder, CO, USA [b] School of Engineering and Physical Sciences, Heriot-Watt University, Edinburgh, UK

First Published:January2009

To cite this Article Stevens, Martin J., H. Hadfield, Robert, Gerrits, Thomas, Clement, Tracy S., Mirin, Richard P. and Nam, Sae Woo(2009)'Infrared wavelength-dependent optical characterization of NbN nanowire superconducting single-photon detectors',Journal of Modern Optics,56:2,358 — 363
To link to this Article: DOI: 10.1080/09500340802322426
URL: http://dx.doi.org/10.1080/09500340802322426

Journal of Modern Optics
Vol. 56, Nos. 2–3, 20 January–10 February 2009, 358–363

Taylor & Francis
Taylor & Francis Group

Infrared wavelength-dependent optical characterization of NbN nanowire superconducting single-photon detectors

Martin J. Stevens[a]*, Robert H. Hadfield[b], Thomas Gerrits[a], Tracy S. Clement[a], Richard P. Mirin[a] and Sae Woo Nam[a]

[a]*Optoelectronics Division, National Institute of Standards and Technology, Boulder, CO, USA;* [b]*School of Engineering and Physical Sciences, Heriot-Watt University, Edinburgh, UK*

(*Received 31 January 2008; final version received 3 July 2008*)

We report optical characterization of NbN nanowire superconducting single-photon detectors as a function of wavelength in the near infrared. System detection efficiency decreases from ~6% at 1.15 μm to ~2% at 1.72 μm, while timing jitter remains relatively constant at ~60 ps full-width-half-maximum over the range 0.7–2.0 μm. We further demonstrate the capabilities of this detector with a time-correlated single-photon counting measurement of photoluminescence from a semiconductor sample emitting at 1.65 μm.

Keywords: single-photon detectors; time-correlated single-photon counting; superconducting devices; infrared photodetectors

1. Introduction

Improved single-photon detectors in the near infrared (NIR) could foster advances in a wide range of scientific and technological applications. For example, fiber-based quantum communications [1,2] would ideally operate at wavelengths around 1.3 and 1.55 μm to take advantage of low-loss optical fibers and the existing telecommunications infrastructure. In biological systems, singlet oxygen is an important intermediary in many processes. The only direct way to detect singlet oxygen is by monitoring its very weak emission at 1.27 μm; time resolved detection of this emission at a single-photon level provides a way to regulate dosage in photodynamic therapy [3]. Time-correlated single-photon counting (TCSPC) is widely used for measuring spontaneous emission lifetimes in solid state, chemical and biological systems, but to date has been limited almost exclusively to wavelengths below ~1.1 μm [4]. TCSPC methods can be used in laser ranging applications at 'eye-safe' wavelengths beyond 1.5 μm [5,6]. Longer wavelengths also offer opportunities for remote sensing of atmospheric greenhouse gases, since carbon dioxide and methane have several absorption bands between 1.57 and 2.3 μm, where the influence of water vapor is weak [7]. In the semiconductor industry, picosecond imaging circuit analysis (PICA) is a valuable method for *in situ*, noninvasive fault testing of high-speed CMOS circuits [8]. Faulty transistors give off a photoemission signature; the wavelength of this signature depends on the gate voltage. Therefore, as components are miniaturized further and gating voltages are reduced, longer wavelength detection is increasingly important.

Progress in these and other NIR photon counting applications has been slowed by the lack of high quality single-photon detectors sensitive to NIR photons. The small selection of photomultiplier tubes that operate in the NIR have very low quantum efficiency. Silicon-based single-photon avalanche diodes (SPADs), which are widely used for visible light, are not sensitive to wavelengths beyond ~1.1 μm. InGaAs SPADs respond to wavelengths up to ~1.7 μm, but suffer from high dark count rates and afterpulsing probabilities, thus they typically require temporal gating and low repetition rates [9–11].

Superconducting single-photon detectors (SSPDs) based on nanopatterned NbN have emerged as strong competitors to these conventional detectors [12–28]. SSPDs are sensitive over a broad range of the optical spectrum from the ultraviolet to the mid-infrared [13,14]. They can be operated at high count rates without temporal gating or afterpulsing [13], and detection efficiencies can exceed 50% for an SSPD embedded in a resonant optical cavity [15]. Unlike that of a conventional Si SPAD, the timing jitter profile of an SSPD has a Gaussian shape, offering a significant advantage in time-resolved measurements, where emission lifetimes must often be deconvolved from

*Corresponding author. Email: marty@nist.gov

ISSN 0950–0340 print/ISSN 1362–3044 online

DOI: 10.1080/09500340802322426
http://www.informaworld.com

raw data [16]. Their low dark count rates, even in ungated operation, have allowed implementation in Hanbury Brown–Twiss interferometry for single-photon source characterization [17–19]. At wavelengths near 1.55 μm, SSPDs have demonstrated their considerable advantages over conventional detectors for monitoring correlated [20] and entangled [21] photon pairs. SSPDs have also been used in secure quantum key transmission at 10 GHz clock rate through a record-setting 200 km of optical fiber [22] and in 'eye-safe' laser ranging experiments at 1.55 μm with sub-centimeter depth resolution [23]. The planar, meander geometry of SSPDs is well suited to fabricating multi-element devices with a high fill factor, offering the potential for fast, large-area devices and the possibility of resolving photon number [24]. The principal drawback of SSPDs is that they must be operated at temperatures near 4 K. However, we have minimized the associated difficulty and expense by packaging several devices in a practical, fiber-coupled, cryogen-free system [17,25].

Here, we report characterization of our fiber-coupled SSPD system over a broad range of the NIR spectrum, encompassing wavelengths from 0.7 to 2.0 μm. We show that the system detection efficiency is largest for short wavelengths, and it decreases monotonically with increasing wavelength. The system timing jitter, by contrast, shows very little change over this wavelength range. To demonstrate the benefit of this wavelength-independent jitter, we perform time-resolved photoluminescence measurements on a semiconductor sample emitting at a wavelength of 1.65 μm.

2. Detector packaging

The SSPD device used here is a narrow, superconducting niobium nitride (NbN) wire embedded in a 50 Ω transmission line. The superconducting track is current biased just below its critical current. When this wire absorbs a photon, it momentarily creates a non-superconducting hot spot. As a result, a small voltage is developed briefly across this resistive section of the track, causing a high-speed voltage pulse to propagate along the transmission line [12,13,26]. Figure 1 shows the SSPD used here, which consists of a 100 nm wide meander line with 200 nm pitch, covering a 10 μm × 10 μm area, which is roughly matched to the mode field diameter of a single-mode optical fiber designed for 1.55 μm wavelength.

Since the superconducting detector must be operated at temperatures near 4 K, we have packaged the device in a practical, cryogen-free system using a commercially available cryocooler. This system, which can accommodate several SSPDs, is discussed in detail in [25]. The cryocooler holds the temperature of the SSPD constant to within a few millikelvin, which is crucial for maintaining stable biasing conditions – and thus constant detection efficiency and dark count rate. A single-mode optical fiber couples light into the cryostat, with the end of the fiber positioned as close as possible to the SSPD. A low-noise current source is used to bias the detector, and commercial, room-temperature rf amplifiers amplify the pulses generated by the detector. A typical amplified voltage pulse is plotted in Figure 2. The key to achieving low timing jitter is to generate an amplified pulse with low noise and a fast rise time. Thus, careful choice of amplifiers with adequate bandwidth and sufficiently low noise figure is crucial. The amplifier used here provides more than 18 dB gain with a noise figure of less than 3 dB over a bandwidth of 500 MHz.

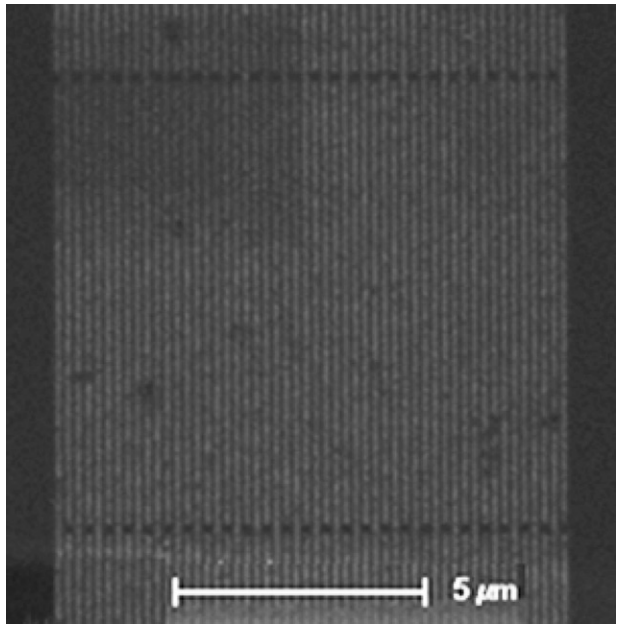

Figure 1. Scanning electron micrograph of the 10 μm × 10 μm SSPD device.

3. Detection efficiency and timing jitter

We use the experimental geometry in Figure 3 to measure both detection efficiency and timing jitter of the SSPD system at a series of fixed wavelengths. To access wavelengths between 1.1 and 2.0 μm, we use ~150 fs optical pulses from a 76 MHz repetition rate optical parametric oscillator (OPO) that is pumped by a Ti:Sapphire laser. To remove light from other sources, the pulse at a given wavelength is spectrally filtered with a grating monochromator and coupled into a single-mode optical fiber designed for 1550 nm

(SMF-28). We use a fiber-coupled optical power meter (not shown) to determine the in-fiber photon flux before the pulse enters the calibrated, in-fiber variable attenuator. This attenuator reduces the flux to < 0.1 photon per pulse by introducing up to 80 dB of attenuation. The pulse then enters the cryocooler in single-mode fiber via an epoxy feedthrough and illuminates the SSPD. For measurements in the 0.7–1.0 μm wavelength range, we bypass the OPO and send the tunable Ti:Sapphire output pulse directly into the monochromator (not shown).

For a particular excitation wavelength, we compute system detection efficiency, DE_{System}, as

$$DE_{\text{System}} = \frac{r_{\text{Total}} - r_{\text{Dark}}}{r_{\text{Photon}}},$$

where r_{Total} is the count rate from the SSPD measured with the timing electronics, r_{Dark} is the SSPD dark count rate measured with the laser blocked, and r_{Photon} is the rate at which photons arrive at the end of the fiber adjacent to the SSPD. r_{Photon} is computed by taking the measured optical power before the attenuator, multiplying by the attenuation factor, and dividing by the photon energy. Results are shown in Figure 4. Detection efficiency is maximum for the highest photon energy (shortest wavelength), and decreases at longer wavelengths.

Previous work has shown that, depending on the device characteristics, an SSPD's detection efficiency can decrease with decreasing photon energy [13,27], or it can be independent of wavelength over a finite spectral range [28]. The results in Figure 4 represent system efficiency, which includes not only the SSPD, but also losses due to fiber transmission and fiber coupling to the device. All three of these processes are potentially wavelength dependent. Note, however, that finding detection efficiency in this way eliminates any inefficiency caused by coupling light from the laser into the fiber – and removes any spectral dependence of optical elements (mirrors, lenses, monochromator) before the fiber launch.

To further characterize this SSPD, we measure its timing jitter using a standard time-correlated single-photon counting (TCSPC) scheme. The output of a fast photodiode triggered by the laser starts a timer, and a voltage pulse from the SSPD stops the timer.

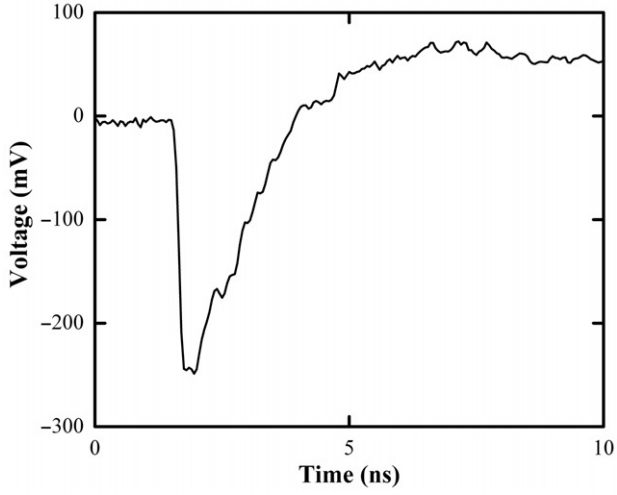

Figure 2. Amplified voltage pulse from the SSPD.

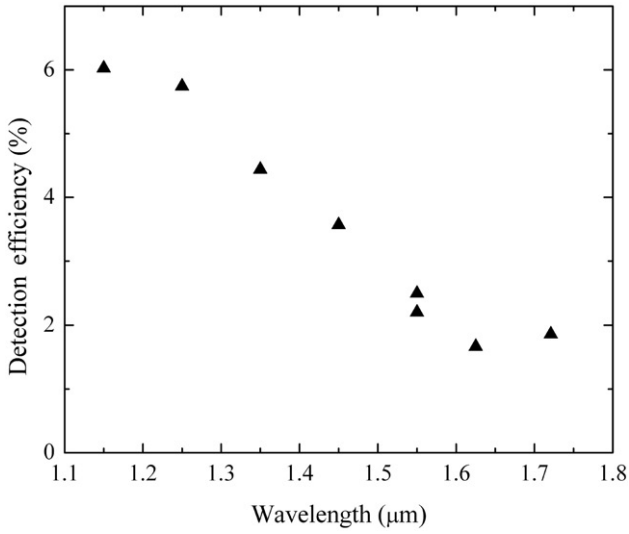

Figure 4. Measured system detection efficiency as a function of excitation wavelength for our fiber-coupled SSPD system. The system detection efficiency contains contributions from the SSPD, the optical fiber, and the fiber-SSPD alignment. The SSPD bias current is constant for all data shown in Figures 4–6.

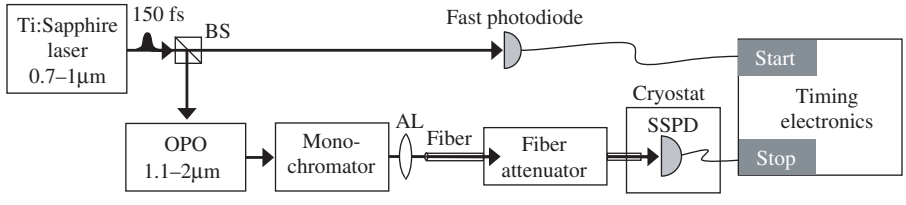

Figure 3. Experimental geometry for measuring timing jitter. BS, beamsplitter; AL, aspheric lens. To determine the system detection efficiency, we measure the optical power in the fiber just before the attenuator with an in-fiber power meter (not shown), correct for the attenuation, and compare to the SSPD count rate measured with the timing electronics.

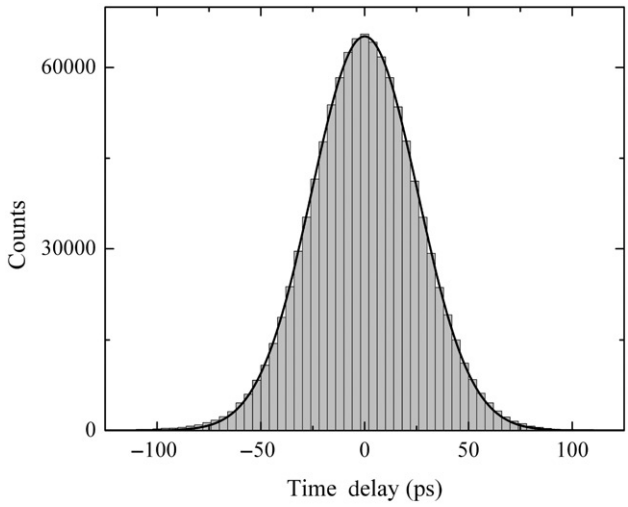

Figure 5. Measured timing jitter histogram for 1.25 μm excitation (gray bars) and a Gaussian fit with 59.9 ps FWHM (solid curve).

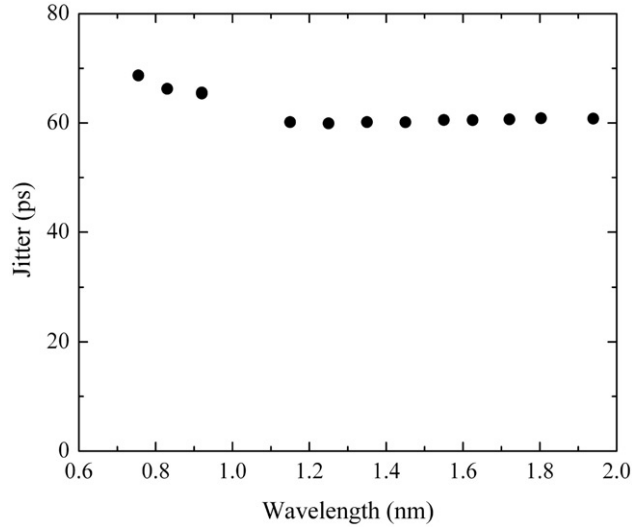

Figure 6. Measured system timing jitter as a function of excitation wavelength.

The time delay between start and stop is stored in a multi-channel analyzer (MCA). This process repeats many times, building up a histogram of start-stop time delays in the MCA. The start rate is the laser repetition rate of 76 MHz, and the in-fiber attenuation is adjusted to keep the stop rate at or below ~100 kHz to ensure much less than one stop per start, preventing a pile-up of counts in the early time bins. In this limit, the measured histogram is directly proportional to the detection system's instrument response function (IRF), provided the optical pulses are much shorter than this IRF. The electronics contribute a timing jitter of less than 30 ps to the measurements; this adds in quadrature with any jitter from the detector and the optical components [4].

Figure 5 shows the measured IRF for 1.25 μm excitation, along with a Gaussian fit with a 59.9 ps full-width-half-maximum (FWHM). Figure 6 plots the result of fits for a series of fixed wavelengths. The jitter, which we take as the FWHM of the IRF, is nearly constant at ~60 ps for all wavelengths longer than 1 μm. The slightly larger jitter observed below 1 μm may be due to modal dispersion, since light at these shorter wavelengths can launch into multiple transverse modes of the fiber. Note that all data in Figures 4–6 are taken with the same SSPD bias current, for which the dark count rate is approximately 650 Hz.

4. Time-resolved photoluminescence

The above results demonstrate that our fiber-coupled SSPD system can be used effectively for time-resolved measurements at a variety of wavelengths in the NIR. Although the detection efficiency decreases at longer wavelengths, there is minimal spectral dependence to the timing jitter. This latter result is particularly useful in TCSPC: typically the only short pulse available for measuring the IRF is the pump – and the pump is often at a very different wavelength than the emission under study. Conventional detectors such as SPADs often have IRFs that depend strongly on wavelength [29], complicating data analysis in this scenario.

Here, we demonstrate the use of an SSPD to time resolve the NIR emission of a semiconductor sample. The sample is an InGaAs epilayer that is lattice matched to InP and has a band gap of ~0.75 eV. When pumped with photons that have an energy higher than this gap, the sample luminesces near the band edge, corresponding to a wavelength of ~1.65 μm. To time-resolve this emission, we use TCSPC in the geometry shown in Figure 7. The sample is optically pumped with a Ti:Sapphire laser that produces ~1 ps pulses with a center wavelength of 780 nm at a repetition rate of 82 MHz. The 1.65 μm photoluminescence (PL) from the sample is collected with an objective lens, spectrally filtered by a monochromator, and coupled into a single-mode fiber for transmission to the SSPD inside the cryocooler. The start rate is 82 MHz, and the stop rate is ~5.5 kHz, clearly satisfying the requirement of $\ll 1$ stop per start. Thus, the histogram generated by the timing electronics is proportional to the time-resolved PL intensity, giving a direct measure of the sample's spontaneous emission lifetime [4].

Figure 8 plots the results of this spontaneous emission lifetime measurement with an acquisition time of just under one minute. Open triangles represent the SSPD system IRF, solid circles show the time-resolved

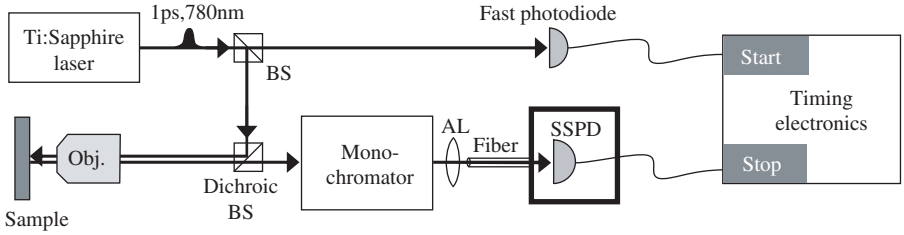

Figure 7. TCSPC experimental geometry where BS, beamsplitter; Obj., microscope objective, and AL, aspheric lens.

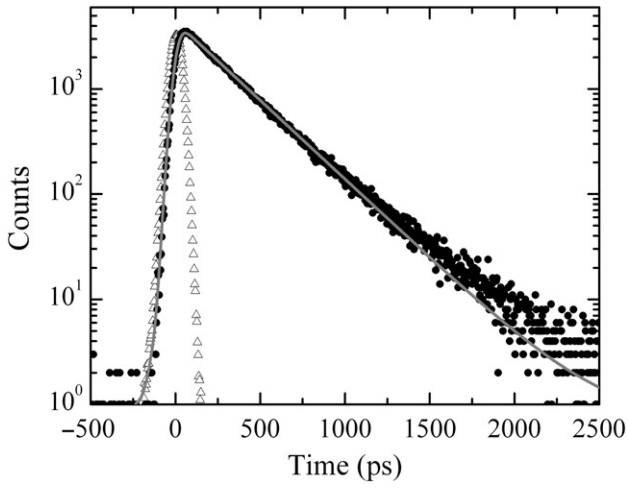

Figure 8. Measured time-resolved PL (solid circles) from an InGaAs epilayer emitting at 1.65 μm. Also plotted are the IRF measured at 780 nm (open triangles) and a fit to the PL data (gray curve). The fit is the measured IRF convolved with a single exponential decay having a lifetime of 290 ps.

PL data, and the solid gray curve is a fit to the decay data. This fit is the measured IRF convolved with an exponential function with a decay constant of 290 ps; thus, the spontaneous emission lifetime of the InGaAs epilayer is ~290 ps. The measured PL data follow the single exponential decay curve very well through more than two decades of dynamic range. The Gaussian temporal response and low dark count rate of the SSPD system enable the excellent signal-to-noise evident in the data.

5. Summary

We have characterized the NIR wavelength-dependence of a fiber-coupled SSPD system. The system detection efficiency decreases monotonically with increasing wavelength, while the system timing jitter remains relatively constant at ~60 ps FWHM. We have demonstrated the system's utility for measuring the spontaneous emission lifetime of an InGaAs sample by time resolving the photoluminescence at 1.65 μm. This fiber-coupled detector system has already been implemented in a number of experiments [16–18, 20–23, 25], and should find use in other applications requiring single-photon sensitivity to NIR light with high temporal resolution and low dark count probability.

Acknowledgements

We thank G. Gol'tsman for providing the SSPD device and A. Holmes for providing the InGaAs epilayer sample. We also thank B. Baek, E. Gansen and K. Silverman for helpful discussions.

References

[1] Gisin, N.; Ribory, G.; Tittel, W.; Zbinden, H. *Rev. Mod. Phys.* **2002,** *74,* 145–195.
[2] Gisin, N.; Thew, R. *Nat. Photonics* **2007,** *1,* 165–171.
[3] Jarvi, M.T.; Niedre, M.J.; Patterson, M.S.; Wilson, B.C. *Photochem. Photobiol.* **2006,** *82,* 1198–1210.
[4] Becker, W. *Advanced Time-correlated Single-photon Counting Techniques;* Springer: Berlin, 2005.
[5] Albota, M.A.; Heinrichs, R.M.; Kocher, D.G.; Fouche, D.G.; Player, B.E.; O'Brien, M.E.; Aull, B.F.; Zayhowski, J.J.; Mooney, J.; Willard, B.C.; Carlson, R.R. *Appl. Opt.* **2002,** *41,* 7671–7678.
[6] Buller, G.S.; Harkins, R.D.; McCarthy, A.; Hiskett, P.A.; MacKinnon, G.R.; Smith, G.R.; Sung, R.; Wallance, A.M.; Ridley, K.D.; Rarity, J.G. *Rev. Sci. Instrum.* **2005,** *76,* 083112-1–7.
[7] Abshire, J.B.; Riris, H.; Allam, G.; Sun, X.; Chen, J.; Kawa, R.; Mao, J.-P.; Stephen, M.; Burris, J.F. *Geophys. Res. Abs.* **2007,** *9,* 10014.
[8] Stellari, F.; Tosi, A.; Zappa, F.; Cova, S. *IEEE Trans. Instrum. Meas.* **2004,** *53,* 163–169.
[9] Ribordy, G.; Gisin, N.; Guinnard, O.; Stucki, D.; Wegmuller, M.; Zbinden, H. *J. Mod. Opt.* **2004,** *51,* 1381–1398.
[10] Liu, M.; Hu, C.; Bai, X.; Guo, X.; Campbell, J.C.; Pan, Z.; Tashima, M.M. *IEEE J. Sel. Top. Quant. Electron.* **2007,** *13,* 887–894.
[11] Itzler, M.A.; Ben-Michael, R.; Hsu, C.-F.; Slomkowski, K.; Tosi, A.; Cova, S.; Zappa, F.; Ispasoiu, R. *J. Mod. Opt.* **2007,** *54,* 283–304.
[12] Gol'tsman, G.N.; Okunev, O.; Chulkova, G.; Lipatov, A.; Semenov, A.; Smirnov, K.; Voronov, B.; Dzardanov, A.; Williams, C.; Sobolewski, R. *Appl. Phys. Lett.* **2001,** *79,* 705–707.

[13] Verevkin, A.; Pearlman, A.; Słysz, W.; Zhang, J.; Currie, M.; Korneev, A.; Chulkova, G.; Okunev, O.; Kouminov, P.; Smirnov, K., *et al. J. Mod. Opt*. **2004,** *51,* 1447–1458.

[14] Gol'tsman, G.N.; Korneev, A.; Rubtsova, I.; Milostnaya, I.; Chulkova, G.; Minaeva, O.; Smirnov, K.; Voronov, B.; Słysz, W.; Pearlman, A., *et al. Phys. Status Solidi (c)* **2005,** *2,* 1480–1488.

[15] Rosfjord, K.M.; Yang, J.K.W.; Dauler, E.A.; Kerman, A.J.; Anant, V.; Voronov, B.M.; Gol'tsman, G.N.; Berggren, K.K. *Opt. Express*. **2006,** *14,* 527–534.

[16] Stevens, M.J.; Hadfield, R.H.; Schwall, R.E.; Nam, S.W.; Mirin, R.P.; Gupta, J.A. *Appl. Phys. Lett*. **2006,** *89,* 031109-1–3.

[17] Hadfield, R.H.; Stevens, M.J.; Gruber, S.G.; Miller, A.J.; Schwall, R.E.; Mirin, R.P.; Nam, S.W. *Opt. Express*. **2005,** *13,* 10846–10853.

[18] Hadfield, R.H.; Stevens, M.J.; Mirin, R.P.; Nam, S.W. *J. Appl. Phys*. **2007,** *101,* 103104-1–7.

[19] Zinoni, C.; Alloing, B.; Li, L.H.; Marsili, F.; Fiore, A.; Lunghi, L.; Gerardino, A.; Vakhtomin, Yu.B.; Smirnov, K.V.; Gol'tsman, G.N. *Appl. Phys. Lett*. **2007,** *91,* 031106-1–3.

[20] Zhang, Q.; Xie, X.; Takesue, H.; Nam, S.W.; Langrock, C.; Fejer, M.M.; Yamamoto, Y. *Opt. Express*. **2007,** *15,* 10288–10293.

[21] Liang, C.; Lee, K.F.; Medic, M.; Kumar, P.; Hadfield, R.H.; Nam, S.W. *Opt. Express*. **2007,** *15,* 1322–1327.

[22] Takesue, H.; Nam, S.W.; Zhang, Q.; Hadfield, R.H.; Honjo, T.; Tamaki, K.; Yamamoto, Y. *Nat. Photonics*. **2007,** *1,* 343–348.

[23] Warburton, R.E.; McCarthy, A.; Wallace, A.M.; Hernandez-Marin, S.; Hadfield, R.H.; Nam, S.; Buller, G.S. *Opt. Lett*. **2007,** *32,* 2266–2268.

[24] Dauler, E.A.; Robinson, B.S.; Kerman, A.J.; Yang, J.K.W.; Rosfjord, K.M.; Anant, V.; Voronov, B.; Gol'tsman, G.N.; Berggren, K.K. *IEEE Trans. Appl. Supercond*. **2007,** *17,* 279–284.

[25] Stevens, M.J.; Hadfield, R.H.; Schwall, R.E.; Nam, S.W.; Mirin, R.P. *IEEE J. Sel. Top. Quant. Electron*. **2006,** *12,* 1255–1268.

[26] Yang, J.K.W.; Kerman, A.J.; Dauler, E.A.; Anant, V.; Rosfjord, K.M.; Berggren, K.K. *IEEE Trans. Appl. Supercond*. **2007,** *17,* 581–585.

[27] Słysz, W.; Wegrzecki, M.; Bar, J.; Grabiec, P.; Górska, M.; Zwiller, V.; Latta, C.; Böhi, P.; Pearlman, A.J.; Cross, A.S., *et al. J. Mod. Opt*. **2007,** *54,* 315–326.

[28] Engel, A.; Semenov, A.; Hübers, H.-W.; Il'in, K.; Siegel, M. *J. Mod. Opt*. **2004,** *51,* 1459–1466.

[29] Krahl, R.; Bülter, A.; Koberling, F. PicoQuant GmbH TechNote MPD SPAD, **2005.** http://www.picoquant.com/products/pdm/technote_pdm.pdf (accessed Oct 31, 2008).